

A Turing-based bimodal population code can specify
Cephalopod chromatic skin displays

Khalil Iskarous*
University of Southern California
kiskarou@usc.edu

Jennifer Mather
University of Lethbridge
jennifermather05@gmail.com

Jean Alupay
Greater Farallones Association
jalupay@farallones.org

*Corresponding Author:
Khalil Iskarous
1538 S. Westgate Ave.,
Los Angeles, CA 90025
kiskarou@usc.edu

Abstract

The skin of a cephalopod forms a dazzling array of patterns made by chromatophores, elastic sacs of pigment that can be expanded by muscles to reveal their color. Tens of thousands of these chromatophores can work together to generate a stable display of stripes, spots, mottled grainy camouflage, or dynamic oscillations and traveling waves of activation. How does a neuromuscular system organize the coactivation of thousands of degrees of freedom through simple central commands? We provide a minimally-complex physiologically-plausible mathematical model, using Turing's morphogenetic equations, that can generate the array of twelve static and four dynamic types of skin displays seen in several cephalopod species. These equations specify how muscle cells on the skin need to locally interact for the global chromatic patterns to be formed. We also demonstrate a link between Turing neural computations and the asynchronous type of computing that has been extensively demonstrated in brain systems: population coding, using bimodal codes, with the relative heights of the modes specifying the kind of global pattern generated. Since cephalopod skins are a "visible neural net", we believe that the computational principles uncovered through their study may have wider implications for the functioning of other neural systems.

Keywords: Cephalopod Displays, Turing patterns, Population Codes, Pattern Formation, Fokker-Planck Equations.

1. Introduction: One of the most spectacular aspects of the biology of the cephalopods is their variable skin chromatic displays (Hanlon & Messenger, 2018). Many animals have an external appearance that is sometimes complex and is adapted to their environment (Bard, 1981), but cephalopods are special in that they have not one but a variety of appearances (Borrelli et al., 2006). They can produce static spots, lines, and patches of different levels of regularity (Figures 1 and 2, Column 1), allowing them to both blend into their environment and at other times to increase their conspicuousness (Cott, 1940; Zylinski et al., 2011). At other moments they can exhibit dynamic traveling waves, flashing and flickering (How et al, 2017; Rosen and Gilly; 2015; Laan et al., 2014). The chromatic displays are produced by the expansion of elastic sacs or chromatophores (Messenger, 2001), and because there is direct neural control of the muscles that expand the sacs, changes in appearance can take place across milliseconds and across areas as small as a square millimeter. Chromatophore density depends on age and species, and Packard & Sanders (1971) estimated that there are hundreds of chromatophores per square mm in the skin of the octopus. So, for an adult cephalopod the chromatic displays are due to a symphony of excitation and relaxation of hundreds of thousands of chromatophore muscles. This very richness offers a problem: how can the contraction and relaxation of hundreds of thousands of these chromatophore muscle units be coordinated to form global patterns with a few stripes, spots, or a traveling wave? How do two far-apart chromatophores, for instance, end up being part of a group of spots, units of a single display, with correlated motor activity? This is an instance of the problem underlying all of animal motor control: how can a high-degree-of-freedom system of muscles be controlled for a low-degree-of-freedom task (Bernstein, 1967)? In this instance, we have hundreds of thousands of countable degrees of

freedom in the chromatophore muscles, and a few degrees of freedom in the display, e.g., the number and direction of lines or the level of coarseness of an irregular pattern. Work on movements of the arm of the octopus has already helped us in understanding how neural systems help solve the degrees of freedom problem (Sumbre et al., 2005; Levy and Hochner, 2017). The question now is whether understanding of chromatic displays can further the solution to Bernstein's (1967) problem (Turvey, 1991), furthering our understanding of motor control in general.

Ishida (2021) has provided evidence for the hypothesis that Turing reaction-diffusion computations could be the basis for the generation of static cephalopod skin displays, and in this paper, we build on this work and provide a mathematically-minimal physiologically-plausible Turing computational model for generating both static and dynamic patterns, and show that these computations can underly a simple bimodal population code model for actual asynchronous neural function. The Turing-hypothesis for how many neural degrees of freedom on a cephalopod skin can coordinate their activities has several precursors. Packard and Sanders (1969) suggested that lateral inhibition, an aspect of Turing computation, is a likely mechanism for cephalopod skin displays. This is a computational mechanism suggested by Mach for edge detection in visual perception, where neighboring neurons (microscopic scale) give each other negative local feedback, resulting in an edge (macroscopic scale) emerging (Oster, 1988). That is, many local computations of the same type (inhibition) result in a global pattern. Packard (2001| 2006) later called this the Horizontal Control Hypothesis: local communication amongst muscle cells in the skin and/or neurons in the higher brain centers

results in the global patterns. Rosen and Gilly (2017) have found evidence of limited local communication between the muscle cells of contiguous chromatophores, making this hypothesis physiologically feasible. Also, Reiter et al. (2018) have provided electrophysiological evidence for simple local communication rules of the inhibitory-surround type that could enable chromatic pattern. But what exactly would the rules of communication amongst muscle cells need to be in order to produce the empirically observed broad spectrum of static and dynamic patterns? The aim of this paper is to provide a minimal mathematical model of local communication amongst cells, myogenic and/or neural, that could generate the observed typology of patterns (Hanlon and Messenger, 1988; Leite and Mather, 2008; Mather and Alupay, 2016; Norman and Debelius, 2000), while agreeing with recent electrophysiological evidence (Rosen and Gilly, 2017; Reiter et al., 2018; Liu and Chiao, 2018; Chung et al., 2020). Our aim is to try to understand what the central motor program actually specifies, as well as the similarities and differences amongst the motor program instructions for different patterns.

Making an explicit formulation of local communication to global pattern formation in cephalopods is important beyond an understanding of these animals, since a cephalopod's skin is a "a 'neural' net that can be seen with the naked eye" (Packard, 2001). Work on this easily visible system can potentially tell us a great deal about how global correlation can arise in a neural system (Cowan, 2014; Wilson and Cowan, 1972, 1973; Buice and Cowan, 2009; Ermentrout and Cowan, 1979; Ermentrout et al., 1986; Botteiger et al. 2007). Evidence has been mounting that correlations can exist across space and time in brains, from varieties of brain waves to communication between motor and perceptual systems (Fernández-Ruiz et al,

2021; Melloni et al., 2007). It is surely the case that global connections between distant brain regions and common excitation of multiple areas from one control area are important contributors to global correlation in neural systems. However, local communication may also have a role, and this could be made clearer by investigating a system such as chromatic display formation where the resulting patterns of correlation can be seen.

The idea that some strategies of local communication amongst units can result in pattern started with Turing's theory of morphogenesis (Turing, 1952; Chua, 2005), which provided a mathematical model of how the same local microscopic interactions everywhere on an initially uniform medium can result in macroscopic forms like stripes or spots on an animal's skin, for instance. Developmental biology now has proven Turing's theories through an extensive list of cases where there is detailed molecular evidence (Meinhardt, 2012; Cooper et al., 2018; Watanabe and Kondo, 2014; Inaba et al., 2020; Newman, 2019) that local protein-mediated interactions, that are on average the same throughout an initially mostly uniform region, are the basis for the genesis of global patterns.

Turing's principle predicts many different possible global patterns in development, as the local interactions can be qualitatively and quantitatively different. In the best studied model for morphogenesis, the domain, or field, has two variables at each point. One variable, the *activator* (A), promotes its own growth, and the growth of the other variable, the *inhibitor* (I), which in turn inhibits the growth of A. This is called the *reaction*. In addition, A's value at each point tends to become closer to the value of A in its local spatial neighborhood (Maxwell, 1871).

This tendency of spatial equalization, or the diminution of spatial discrepancy, is also true for I, and is called *diffusion*. Note the *locality* of the computation in this model: the reaction of A and I occurs at each point, and the diffusion relates each point only to its immediate neighbors. These reaction-diffusion systems can have very different functional forms (Murray, 2001). For instance, in some systems A's self-promotion or promotion of I is linear, increasing A or I equally for equal increases of A, and in other systems the reaction could be sigmoidal, with great I increases for small-magnitude increases of A, and hardly any change in I for large-magnitude increases of A. Also, given the functional forms of the reaction, the degree to which I inhibits A, or A promotes itself, for instance, is a variable parameter, a coefficient. Therefore, each qualitatively different reaction-diffusion model can take an infinite number of quantitatively different forms, and the functional forms of the reaction, as well as the coefficients determine the resulting global pattern, and whether it is structured (e.g., spots or stripes) or not (uniform).

Turing's surprising insight was to establish the mathematical conditions under which the same purely local interactions throughout the medium can result in stable structured global patterns where there is a relationship between the activator values at arbitrary spatial separation within the medium (Turing, 1952). The most important of these conditions is that the speed of equalization of I in a neighborhood is greater than the speed of A equalization, a condition that is highly consistent with lateral inhibition suggested for chromatic pattern formation in cephalopods by Packard and Sanders (1969). Turing also knew that reaction-diffusion media can exhibit temporal long-time correlation through *oscillation* of the values of A and I, a system

studied in great detail by Hopf (Walgraef, 1997), as well as spatiotemporal correlation through traveling waves of the activator (Cross and Hohenberg, 1993), but he thought that three reactants are necessary to realize time-varying patterns. The more general Turing-Hopf model we will discuss in this paper establishes how spatial, temporal, and spatiotemporal order could arise in an initially mostly homogeneous medium, without long distance connections or neurons that directly correlate spatially or temporally distant activations (even though such connections can exist and influence resulting global patterns).

In neuroscience, local computation was developed by Cowan and his colleagues as the basis of a *neural* morphogenesis, where global brain patterns are explained by local computations amongst excitatory and inhibitory neurons (Wilson and Cowan, 1972, 1973; Oster, 1988). Indeed, Cowan (2014) has shown that Turing bifurcations are a main cause of global neural correlations. Such computation has been used to predict visual hallucination patterns (Ermentrout and Cowan, 1979), global patterns of neural activation in visual cortex due to local computations, and molluscan shell pattern formation (Meinhardt, 1982; Ermentrout et al., 1986). Botteiger et al. (2009) (Appendix E) suggest that such a model can also explain dynamic cephalopod chromatic displays, and Meinhardt (1982) collaborated with Andrew Packard, informally, to suggest that lateral inhibition can be implemented in a Turing-type reaction-diffusion equation to explain developmental patterns of chromatophore formation (Packard, 2001). Recently Ishida (2021) has shown that Turing pattern formation is indeed a plausible hypothesis for the formation of static cephalopod skin displays by employing a 2D Cellular Automaton model that performs local computations resulting in global patterns, in combination

with a Convolutional Neural Network modeling the perceptual system and that extracts parameters from visual scenes that can drive motor pattern formation. In this paper, we give further evidence for Ishida's (2021) Turing-hypothesis by proposing and solving a mathematically-minimal physiologically-plausible Barrio-Varea-Aragón-Maini model (Barrio et al., 1999) that can generate both static and dynamic patterns, then show how an asynchronous bimodal population code could be extracted from this model. This last step is important, since actual brain systems have long been known to be stochastic and asynchronous in their functioning (von Neumann, 1956; Cowan, 2014), therefore hypotheses about neural computational need to specify how a neural system will implement the computation through stochastic and asynchronous firing. In Section 2 we propose a minimal Turing morphogenetic model, the Barrio-Varea-Aragón-Maini model (Barrio et al., 1999), also called the BVAM model, and argue for its physiological plausibility. In Section 3.1., we show how the BVAM system predicts the spectrum of observed static cephalopod displays, and show how variation in the system coefficients leads to display changes. In Section 3.2., we build on the work of Marquez-Lago and Padilla (2014) to show that it's possible to derive a bimodal population code from the BVAM system, which can be simulated via a Fokker-Planck Equation, and that the relative heights of the modes lead to variation in the skin patterns in a systematic way. We believe that this is an important result, since actual brain systems (whose actions for these animals are seen on their skin (Packard, 2001)) are stochastic and fire asynchronously, so for a Turing computational pattern to be actually implementable in a neural system, a stochastic asynchronous embodiment is necessary. Section 3.3 then shows how the BVAM system also

generates time-varying patterns on the skin. A brief discussion and conclusion are then presented in Section 4.

2. Methods: The general form for the Reaction-Diffusion (RD) system described earlier is:

$$\begin{aligned}\frac{\partial A}{\partial t} &= f(A, I) + D_A \Delta A \\ \frac{\partial I}{\partial t} &= g(A, I) + D_I \Delta I\end{aligned}\quad (1)$$

The left-hand sides of the equations represent the temporal change of the Activator A and Inhibitor I, respectively. The first terms on the right-hand sides, f and g, express the reaction functions, how A and I influence each other, and the Δ express the discrepancy between A and I at a point vs. the values in their immediate surroundings (Maxwell, 1871). The Ds are the speeds with which A and I equalize with their local environments. Therefore, the change in each of the variables depends on themselves, the other, and their spatial neighbors. Again, there is an infinite number of such systems due to the infinitude of possible f and g functions and the infinitude of the coefficients of the reaction and diffusion. Our goal is to determine the simplest RD equation that can generate the repertoire of cephalopod chromatic patterns. The search for the simplest model is not due to a belief that natural neuromuscular systems are maximally efficient and non-redundant, since all evidence points to the contrary. As von Neumann (1956) already knew, fault-tolerance and speed can be gained by increase in redundancy of computation. Rather, we seek the simplest system, to know what the *essential* aspects of the neural model for generating the static and dynamic patterns must be like. If we know that, we have bounded the possible models from below in complexity. Knowledge of the minimal kinds of interactions that could generate the patterns could then serve to guide hypothesis generation for electrophysiological and biochemical studies, which are necessary for obtaining

the right physiological realization of the model. This happened in the study of fish chromatic displays, where early theoretical work (Kondo and Asai, 1995) guided work on protein interactions that instantiate the reactions (Watanabe and Kondo, 2014; Asai et al., 1999).

Our search for the simplest model is guided by three results in work on RD systems: 1) quadratic and cubic terms in the reaction are necessary if both spots and stripes are to be generated (Ermentrout, 1991; Shoji and Iwasa, 2003); 2) presence of quadratic and cubic terms can actually generate moving patterns (Barrio et al, 1999; Liu et al, 2007), even when there are only two variables defined at each point (cf., Turing, 1952); 3) Newton, Taylor, and Morse have argued that all nonlinear functions have a linear, quadratic, and cubic components of some magnitude which, when summed, yield some of the simplest qualitative behaviors of the nonlinear functions. So, if we are unsure of what the forms of f and g are, it's best to start with these, as sigmoidal and other functions can be approximated locally using polynomials of the lowest order. Barrio, Varea, Aragón, and Maini (BVAM) argued for the simplest model (Barrio, et al., 1999), in which the first step is to carry out a Taylor-expansion of the f and g functions, and curtailing after the cubic term, yielding terms of f and g proportional to: A , I (linear), A^2 , I^2 , AI , (quadratic), and A^3 , I^3 , AI^2 , IA^2 *cubic. The second step is to make the system even more minimal by eliminating the non-interactive quadratic and cubic terms (A^2 , I^2 , A^3 , I^3), and leaving only one of two interactive cubic terms (eliminating IA^2). The BVAM equations are (Barrio et al., 1999):

$$\begin{aligned}\frac{\partial A}{\partial t} &= g(A + aI - CAI - AI^2) + D_A \Delta A \\ \frac{\partial I}{\partial t} &= g(HA + bI + CAI + AI^2) + \Delta I\end{aligned}\tag{2}$$

The model has 6 parameters g, a, b, H, C, D_A that tune the reaction and diffusion computations. The g parameter tunes the overall size of the pattern, while parameters a, b, H tune the linear interaction (how the A and I change themselves and each other). The parameter C tunes the quadratic interaction of A and I , while D_A , which is less than 1, expresses how slow the diffusion of A is, with respect to the diffusion rate D_I , which is normalized to 1. This is the simplest interactive local computation system, with quadratic and cubic interactions, the simplest nonlinear functions. Is this minimal system enough to generate the variety of static and dynamic patterns? In the next section, we will demonstrate that it is.

The physiological meaning of the A and I variables is not known for certain, but Packard (2006) has suggested that horizontal control could be realized through Calcium-based waves of activation. Indeed, the electrophysiological/biochemical literature on both myogenic and neural cells is compatible with the possibility that A could be the cytoplasmic concentration of Calcium Ca^{2+} , and that I could be a variable controlling the impedance to the rise of cytoplasmic Ca^{2+} , such as Ryanodine receptor concentration (RyR1) (Plummer et al., 2011; Keener and Sneyd, 2009). This suggestion is due to the fact that muscle cell activation is accompanied by a rise in cytoplasmic Ca^{2+} , and that Ca^{2+} is a self-promoter, as would be required of A . Indeed, the fundamental reaction between Ca^{2+} and its inhibitors like RyR1, usually termed Calcium-Induced Calcium Release (CICR), is a pattern generation mechanism which operates in nature

from ultraslow time scales, such as in calcium waves in the egg, to ultrafast, such as myocardium contraction, operating a billion times faster, and it can generate static structured patterns, oscillation, and traveling waves (Jaffe, 2008). In addition, Ca^{2+} pattern formation is involved in both muscle cell contraction, Ca^{2+} the contractile machinery, as well as in neural cells, where Ca^{2+} spikes are the signal necessary for neurotransmitter vesicle docking and exocytosis. So, whether the pattern forming communication is in the skin or in the Chromatophore and Lateral Basal Lobes (Messenger, 2001; Packard, 1995), this is a mechanism that could be involved. It is true, as Rosen and Gilly (2017) have pointed out, that the exact calcium-based mechanism involved in cephalopod chromatic pattern formation is not clear, which is why the model we are providing can be seen as a phenomenological one.

3. Results

3.1. Static Repertoire: Cephalopods are capable of enormous variation in the patterns they can have on their skin, as seen in the first columns of Figure 1 and 2, similar to how human sentences can vary enormously. Yet, just as with language in which there is a much more limited number of constructions or rules of grammar (e.g., active, passive, cleft, subordination), experts in the chromatic behavior of cephalopods have used terms like lines, spots, reticulate, blotch, mottle, and uniform to describe general classes of static patterns (Hanlon and Messenger, 1988; Mather and Alupay, 2016). Lines can be relatively straight lateral bars or antero-posterior stripes (Figure 1a), or the stripes can intersect and be more curved (Figure 1b). The lines can also occur next to spots (Figure 1c). Another simple pattern is regular spots that are either light (inactivated chromatophore muscles) on dark (activated chromatophore

muscles) (Figure 1d) or dark on light (Figure 1e). As irregularity increases and disruptiveness decreases, the lines can be quite short and at angles to each other, which are usually called *reticulate* (Figure 2a). The spots can also be highly irregular polygons or ovals, usually called *blotch*, and these ovals/polygons can be dark on light (Figure 2b) or light on dark (Figure 2c). As irregularities increase, the scale becomes even smaller, and we get patchy textures of variable grain (Figures 2d, 2e), usually called *mottle*. It is also possible to have the entire animal be uniform light (Figure 2f) or dark (Figure 2g). Again, a great deal of variation exists, but we believe that these classes of static patterns represent the consistently described ones in the extensive literature on cephalopod chromatic patterns. The only ones not described here are strictly local, like the eye bar.

The second columns of Figures 1 and 2 provides simulations of each of the static patterns in the first column. The initial condition of the field is random noise, so each time a simulation is run, the exact pattern will be slightly different, but will be within the class represented. The match of the simulation and natural pattern are not intended as exact but as suggestive of the class. The numerical simulations are described in Appendix A. The first 11 rows of Table 1 provide the coefficients of the reaction-diffusion equations for the simulations in the second column of Figures 1 and 2. As can be seen, for the non-uniform static patterns, only two of the parameters, the quadratic parameter C and the Diffusion parameter D need to change in order to obtain the basic static typology. This establishes a minimum of the information that needs to be provided by the higher centers such as the optic lobe to lower pattern formation centers for a particular pattern to be activated (Liu and Chiao, 2017). Moreover, the central commands, if

they provide information as represented in the numbers C and D are quite simple, as they are uniform instructions for purely local communication within the skin or lower brain centers such as the Chromatophore and Lateral Basal Lobes (Packard, 1995), which when performed results in the global chromatic patterns.

But how, specifically, does variation in C and D alter the global pattern? As can be seen from Table 1, as the magnitude of C increases from 0 to 1, patterns change from more line-like to more spot-like, with the polarity of C distinguishing whether the background is dark or light, respectively. And as D_A decreases, irregularity increases. To further understand the global pattern as a function of C and D variation, the third column of Figures 1 and 2 provide the 2D Fourier spectrum (2DFT) of each pattern, which is described in Appendix B. The 1D spectrum has been a very useful quantitative device in the empirical research on cephalopod patterns (Chiao, et al., 2010), and we believe that the additional information in the 2DFT (Zylinski et al., 2011) furthers the use of spectra in the description and comparison of patterns. The center of the 2DFT display expresses the lowest frequency of variation, and the height of the peak there indicates the prominence of a uniform light or dark aspect to the display (e.g., third column of Figure 2, f and g). As spatial frequency variation in a pattern increases, there is more energy seen further and further radially outwards. As can be seen from the third column, lines and spots have peaks at relatively low frequencies, and exhibit very little high frequency energy. Irregular patterns have a wider ring of higher frequencies excited. This agrees with the results of Hanlon et al. (2009) in that it is possible to spectrally distinguish the more *disruptive* patterns like lines and spots as low frequency from the less disruptive ones like mottle, which are higher

frequency. The spectral understanding is furthered in the 2DFT, however, since we can distinguish nicely *within* the class of disruptive: lines show localized excitation on the low frequency ring, whereas spots show more distributed excitation on the low frequency ring, as can be seen by comparing Rows a vs. d and e in the 2DFT column of Figure 1. And as explained in Appendix B, the 2DFT clarifies the superpositional structure of displays, investigated by Anderson et al. (2003) and Kelman et al. (2006), allowing us to see spots as a superposition of stripes, for instance.

As C and D change by small amounts, we sometimes have small changes within a class, but other small changes switch the pattern to a new class entirely. Figure 3 shows entire regions of the D-C space that give basically the same pattern, with small variation. The exact location of the boundaries between the regions depends on the random noise that the simulations start with. Appendix A provides the details on how Figure 3 was generated. The two important generalizations based on Figures 1 and 2 nicely emerge from Figure 3: 1) As D_A increases in magnitude, disruptiveness increases, and irregularity decreases. 2) As C increases in magnitude, the more patterns become more spot-like. The first generalization makes sense, since in the disruptive patterns, like large spots and long stripes, there needs to be large correlation of activation among chromatophores that are far apart, and a higher D_A allows greater speed of spread and therefore further reach from one spot to others. The spectral effect of diffusion can also be seen in Figure 4a, where the normalized amount of low spatial frequency energy was divided by the normalized amount of high spatial frequency energy for each of 2500 simulations, and plotted as a function of D, with C held fixed at different values indicated by the

different rainbow colors. As can be seen, as D_A falls the high spatial-frequency components rise, as expected.

3.2. Bimodal Population Codes: To explain the second generalization, how C-magnitude increase leads to spots, we need to rely on the recent methods of Marquez-Lago and Padilla (2014). If we imagine the intensity of A on the x-axis of a graph, e.g., as in Figure 4c or 4d, with the y-axis representing the probability of that intensity A, a bimodal distribution would indicate that there are two intensities that are quite stable and highly probable. In the blue curve of Figure 4c, one intensity of $A = 1$, which is dark/activated, is highly probable, while another intensity, -1 light/unactivated, is also probable, but less so. If this blue probability curve is interpreted as the probability distribution for the intensity of activation of *any* chromatophore's muscles, then the most probable chromatophore intensity would be $A = 1$, so most chromatophores would be dark, and therefore we would say that the *background* brightness is dark. The less probable light A would be the less frequent intensity, which if we add the additional constraint that nearby chromatophores have similar activation, would therefore be the brightness of *foreground* light spots on the dark background. Note that more probable is identified as background, and less probable as foreground (cf. figure/ground distinction in perception). Therefore, if the instruction to muscle cells is to fire or not independently based on the blue probability distribution in Figure 4c, and we add the additional constraint of common activation of nearby chromatophores (through diffusion), then the observed global pattern would be dark background with light spots (Figure 1d). If the two probability modes become more and more equal, as in the red curve in Figure 4c, the distinction between foreground (less probable) and background (more probable) is blurred, and we get stripes. Marquez-Lago and

Padilla (2014) show that as the quadratic parameter C in a reaction-diffusion system varies, it's as if the associated Boltzmann probability distribution of the activator varies in the way presented in Figure 4c, with the two modes becoming more or less equal to each other. Figure 4d shows the probability distributions leading to a light background with dark spots (Figure 1e). In this explanation, C is the skewness of the bimodal distribution. The fact that the distribution is bimodal to start with is due to the cubic term in the reaction-diffusion system. We believe that the Marquez-Lago and Padilla (2014) interpretation of the quadratic and cubic parts of the reaction-diffusion pattern formation device is quite useful from the neural perspective.

In the analysis of real brain systems, it is known that neurons are not deterministic systems whose synchronous firing (or not firing) is updated by a central clock. Therefore, for a computational system to be physiologically feasible, we need to know something about the probability distributions of the firing of neural populations. The Marquez-Lago and Padilla correspondence between Turing systems and bimodal probability distributions is quite useful. Indeed, we interpret the parametrizable bimodal distributions to be population codes (Dayan and Abbott, 2001). In such a code, each motor state of the system has a probability of being realized. Here the motor states are the degree of activation of muscles of a single chromatophore or a small population thereof. Neurons fire or not according to these bimodal distribution with centrally-specified parameters like skewness C that specify the relative heights of the modes. There is an additional constraint that small populations fire similarly to their neighbors, which is the diffusion effect. Most of the literature on population codes focuses on single-mode distributions, but bimodal distributions have also been investigated (Zemel et al., 1998).

Marquez-Lago and Padilla (2014) show a way of translating from reaction-diffusion systems to Fokker-Planck equations whose solutions are these Boltzmann distributions, discussed in the previous paragraph. We used the Langevin method of simulating the Fokker-Planck equations for the BVAM equations 2, via Euler-Maruyama discretization (details in Appendix C). In these simulations, we solve a Langevin stochastic differential equation with noise determined by the diffusion coefficients and bias determined by the reaction terms (Rajotte, 2014), and the probability distribution of A at convergence is recorded at convergence for 10000 simulations of the same stochastic differential equation. The resulting histograms of A at convergence as C and D are varied in Table 1 are in the fourth columns of Figure 1 and 2. As expected, the spot-like patterns have large skewness, while the line-like patterns have lower skewness. Figure 4e shows the calculated Pearson Skewness histograms from Langevin-simulations with fixed D_A and varying C from -1 to 1. The skewness of the empirical histograms of pixel intensity in the reaction-diffusion simulations such as those in Column 2 of Figures 1 and 2 is also shown. Both vary from high to low skewness, as expected, but one surprising result was that the Langevin-based skewness crossing point was at $C = -.4$, not $C = 0$, as expected. We have eliminated the possibility that this is due to the specific D values used. We believe that this discrepancy is due to the linear components of BVAM, but we leave this for future investigation. To further support the Marquez-Lago and Padilla (2014) interpretation, we also measured the normalized fundamental frequency, F_0 , at the center of each 2D Fourier transform, as energy at that frequency indicates a constant background. As can be seen in Figure 4b, as C varies, with D fixed at various values indicated by different rainbow colors, F_0 drops as the magnitude of C

drops, indicating that spot-like patterns have a pronounced constant background, while stripe-like patterns don't.

3.2. Dynamic Repertoire: When the linear parameters a , b , and H in the BVAM Equation 2 are changed, it's possible for spatiotemporally complex patterns to arise (Leppanen, 2003; Liu et al, 2007; Varea et al., 2007) through Hopf bifurcations (Walgraef, 1997) and interactions of Turing and Hopf patterns. There has been extensive analysis of the spatiotemporal patterns of BVAM (Leppänen, 2004, Varea et al., 2007), and we do not seek to repeat that analysis here. Our goal is to show how different parameter settings in BVAM can lead to the empirically observed dynamic patterns (Laan et al., 2014; Rosen et al., 2015; How et al., 2017). The last four rows of Table 1 show specific parameter settings for producing synchronous flashing, asynchronous flickering, a traveling pulse (Passing Cloud, Mather and Mather, 2004), and periodic traveling waves (Laan et al., 2014; How et al., 2017). Figure 5a shows the mean intensity of all pixels in a field when H is positive and it can be seen that mean intensity oscillates for a few cycles, suggestive of synchronous flashing (Rosen et al., 2015; How et al., 2017). It should be noted that the diffusional constant D_A is quite small, as compared to $D_I = 1$, still consistent with the lateral inhibition communication between units. An easy way for making the oscillation last longer would be to make the two diffusion constants equal, as we see in Belusov-Zhabotinsky limit cycle oscillation of entire media (Walgraef, 1997). Since we wanted to fully explore the dynamical capabilities of a lateral-inhibition medium, we have maintained the diffusion constants to be similar to those seen in the static pattern, which is why the oscillation is short-lived. Of course, long term oscillation could be achieved by issuing the same central command

many times. Figure 5b shows the individual pixel color of three pixels spanning the field. It can be seen that, even though there is a phase difference, the pixels go up and down in intensity quite similarly. Figure 5c shows the oscillation of the same three pixels, when H has increased. Now the three pixels are performing quite different oscillations, i.e., suggestive of asynchronous flicker.

To simulate a traveling pulse (Passing Cloud), we used the same parameters as we did for synchronous oscillation, but instead of using random initial conditions, we used an initial stripe. As can be seen in Figure 5d, the initial stripe at the bottom travels upwards¹. Periodic traveling waves, often seen on cuttlefish, can also be simulated, as seen in the close-up pictures in Figure 5d and 5e, which show 2 different consecutive cycles of a wave. Therefore, the dynamical patterns observed can also be generated through manipulation of only the same six parameters necessary for the static cases, and maintaining the larger D_I than D_A , and the lateral inhibition principle.

4. Discussion and Conclusion: In this paper we have provided further evidence that the Horizontal Control Hypothesis is a possible pattern generation mechanism for chromatic displays of cephalopods. We have sought to provide the simplest concrete instantiation of those rules via Turing-Hopf pattern formation theory using the BVAM universal simplification of

¹ However, since we have used periodic boundary conditions, which reduces boundary artifacts (de Witt, 1996), as compared with zeros-derivative boundary conditions, a part of the stripe travels down from the top of the domain. This artifact of simulation is less harmful than the introduction of aspects of the pattern due to the zero-derivative BCs.

nonlinear reaction-diffusion equations. We have shown that the Horizontal Control Hypothesis specifies interactional parameters for each cell, and furthermore, these interactional parameters can be the same throughout the skin. The Marquez-Lago and Padilla (2014) interpretation of the C parameter further enhances our neural interpretation of the horizontal control hypothesis for the static patterns by suggesting that what is centrally specified is a bimodal probability distribution for firing, together with a constraint that nearby units fire together. We believe that the present work has import for the empirical study of cephalopod patterns (Osorio, 2014) as the higher-level interaction parameters can be used to robustly quantify pattern similarity and differences. We also believe that the work has implications for electrophysiological and biochemical work on cephalopod chromatic displays, as the reaction-diffusion mechanisms we have discussed could guide the search for the biochemical events instantiating them, as has happened in the study of developmental fish skin patterning (Asai et al., 1999).

In earlier work, Iskarous (2019) used the BVAM equations to derive the macroscopic patterns in another behavior in an animal widely separated in evolution from cephalopods: speech in humans. In the latter, the patterns are the gestures of the tongue that specify the consonants and vowels of a language. That work shows that a neural system operating under a BVAM system of equations with Turing-Hopf bifurcations can generate several empirically verified signatures of vocal tract action. Our work on cephalopods is inspired by dynamical work on speech production in the Articulatory Phonology framework (Fowler et al., 1980; Browman and Goldstein, 1989; Saltzman and Munhall, 1989). We feel that this work on the octopus will allow

further progress in our understanding of speech gestures, for example. A common mathematical vocabulary for different animal behaviors helps the cross-fertilization of methods and results across widely different fields of animal behavior, such as the locomotion of nematodes and gaits of many animals (Golubitsky et al., 2004). Advances in mathematical biology, which started with Turing, have had major influence on our understanding of animal development. These could also guide the development of a of minimal mathematical language for describing the vast diversity of animal action, perception, and perhaps even cognition, since in all of these there are local computations and global patterns.

Conflict of Interest: The authors have no conflict of interest to declare.

Acknowledgements: This research was possible due to funding by NSF grant 1246750. We would like to thank Tatiana Leite, Louis Goldstein, and the late Roland Anderson for helpful discussions.

Captions

Figure 1: Disruptive Cephalopod skin displays. Column 1: Pictures of displays on the skins of cephalopods. Column 2: BVAM reaction-diffusion simulations of the displays. Column 3: Two-dimensional Fourier Spectra of the simulations. Column 4: Simulations of Fokker-Planck stochastic versions of the BVAM equations for studying pattern selection. Row 1: Lines (*Octopus chierchiae*; Photo: Roy Caldwell). Row 2: Irregular Stripes (*Octopus chierchiae*; Photo: Roy Caldwell). Row 3: Stripes and spots (*Octopus chierchiae*; Photo: Roy Caldwell). Row 4: Light on Dark Spots (*Sepia pharaonis*; Photo: Authors). Row 5: Dark on Light Spots (*Sepia pharaonis*; Photo: Authors) (Color Online).

Figure 2: Nondisruptive Cephalopod skin displays. Column 1: Pictures of displays on the skins of cephalopods. Column 2: BVAM reaction-diffusion simulations of the displays. Column 3: Two-dimensional Fourier Spectra of the simulations. Column 4: Simulations of Fokker-Planck stochastic versions of the BVAM equations for studying pattern selection. Row 1: Reticulate (*Octopus chierchiae*; Photo: Roy Caldwell). Row 2: Light on dark Blotch (*Abdopus sp.*; Photo: Authors). Row 3: Dark on Light Blotch (*Octopus insularis*; Photo: Tatiana Leite). Row 4: Dark Mottle (*Octopus chierchiae*; Photo: Roy Caldwell). Row 5: Light Mottle (*Abdopus sp.*; Photo: Authors). Row 6: Uniform Light (*Abdopus sp.*; Photo: Authors). Row 7: Uniform Dark (*Octopus chierchiae*; Photo: Roy Caldwell) (Color Online).

Figure 3: D-C typology of patterns. Results of k-means clustering of 2500 simulations based on varying D and C of the BVAM equations (Color Online).

Figure 4: Quantification of deterministic and stochastic models of the skin displays. D controls the amount of high-frequency vs. low-frequency in the 2D Fourier Transform (a). C controls the prevalence of a background, as measured by the fundamental or central frequency (F_0) of the 2D Fourier Transform (b). Bimodal Distributions, with highest peak corresponding to background and lower peak to foreground patches, where the background can be dark (c) or light (d). The skewness of bimodal Boltzmann distributions resulting from Langevin-simulations of the Fokker-Planck version of BVAM (red) and the deterministic simulations (blue) (Color Online).

Figure 5: Dynamic Simulations. The H variation away from $H = -1$ is crucial in switching from static to dynamic patterns. Mean pixel value for two values of H (a). Synchronous flashing is indicated by co-varying values of pixels from 3 different regions of the field (b). Asynchronous flickering is indicated by randomly varying, but oscillatory, variation of pixel values from the same 3 different regions of the field (c). Five frames from a traveling pulse of activation (Passing cloud) (d). Two cycles of variation of a periodic wave train (close-up) resulting from a spiral wave (e and f) (Color Online).

Table 1: Values for BVAM parameters for the static and dynamic simulations that generate the different types of pattern (Color Online).

Figure 1

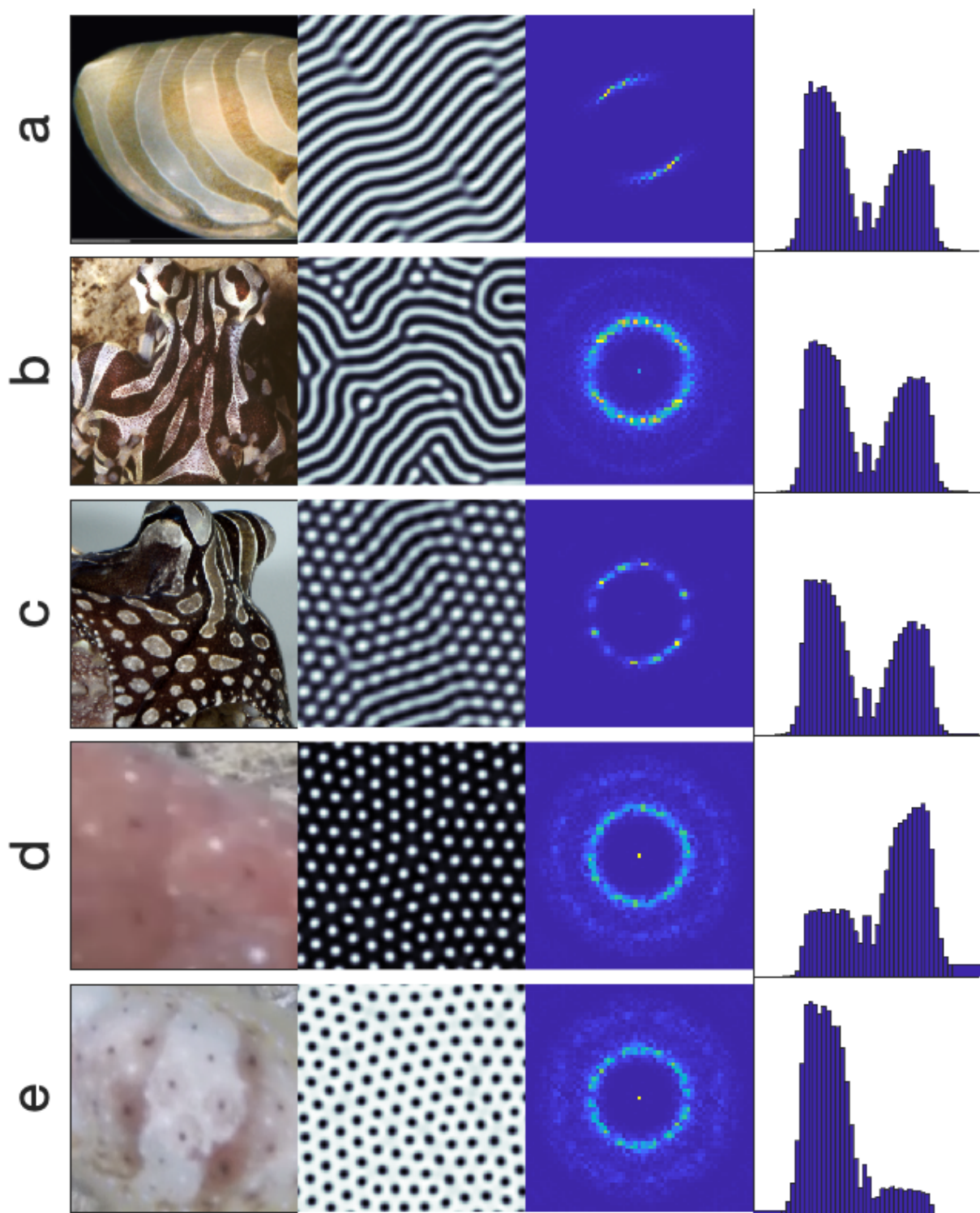


Figure 2

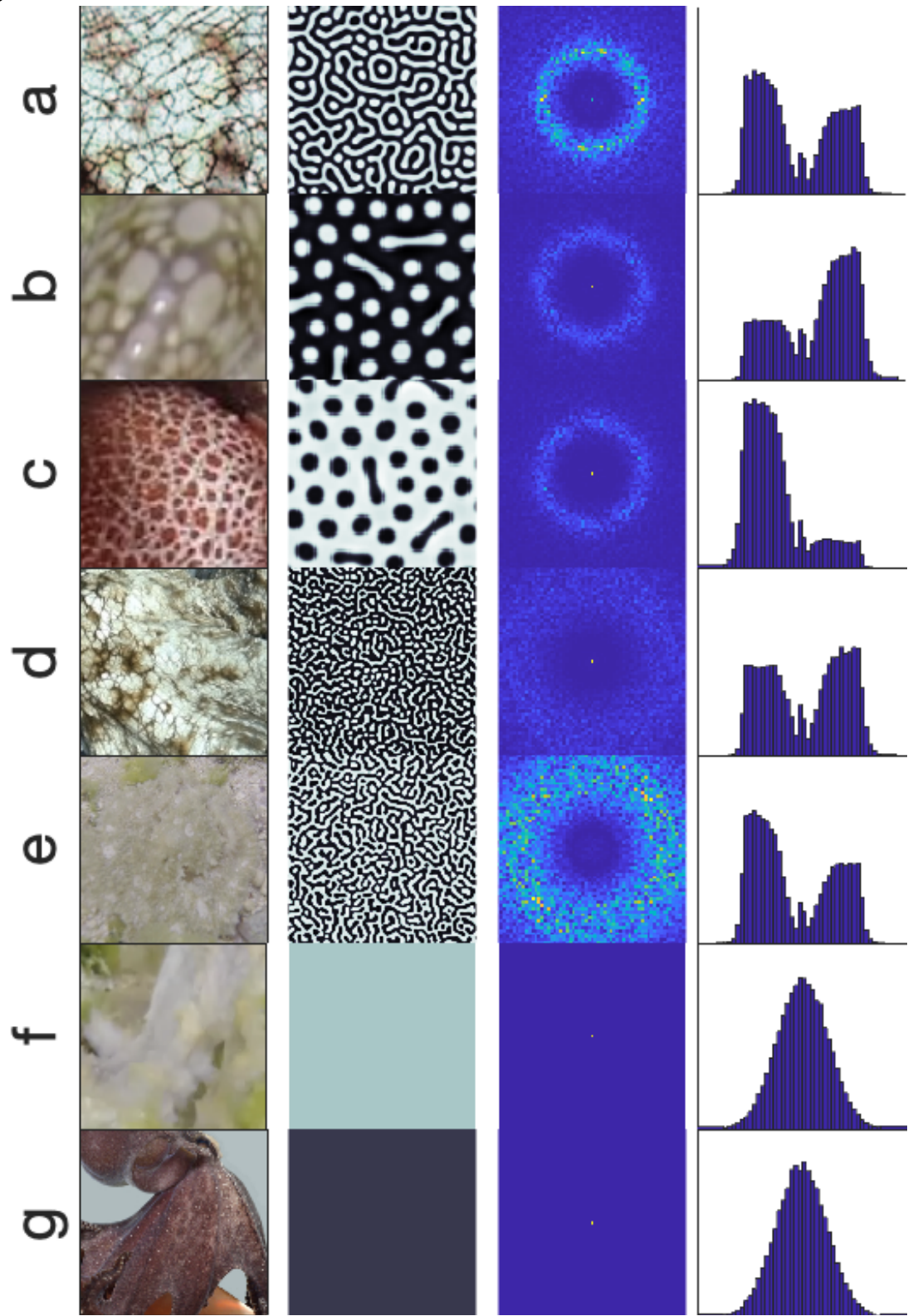


Figure 3

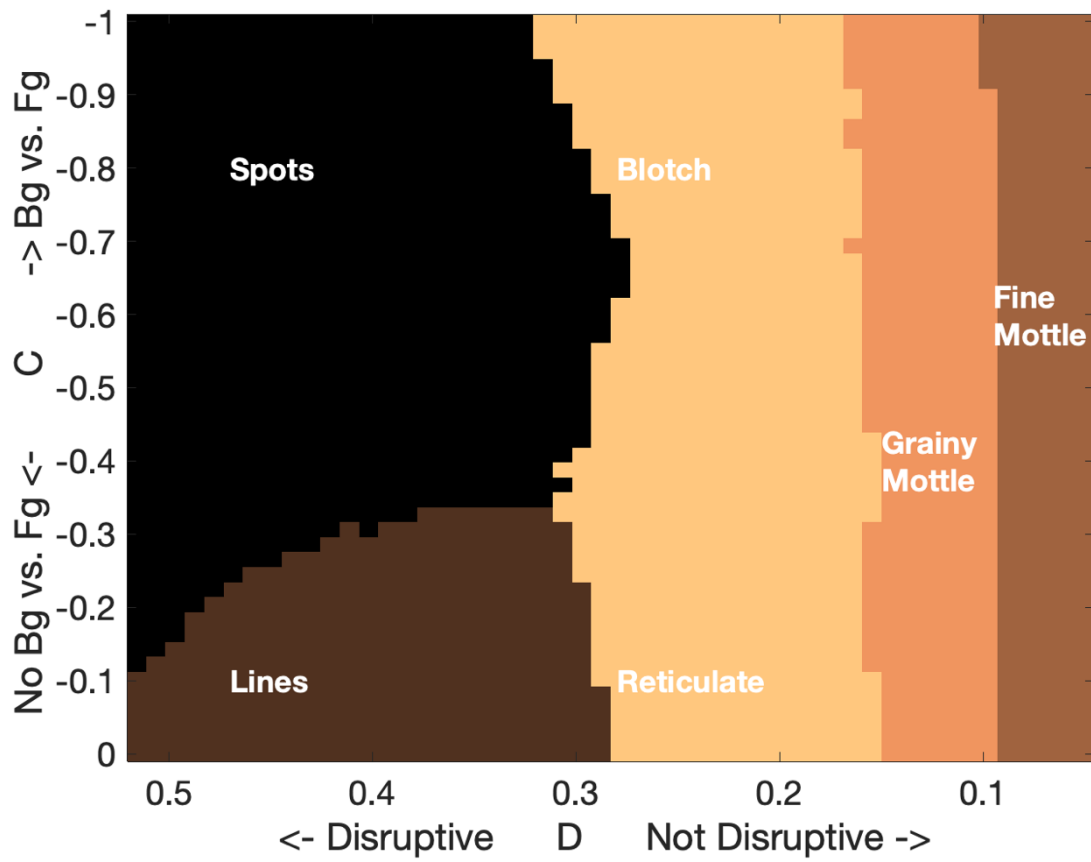


Figure 4

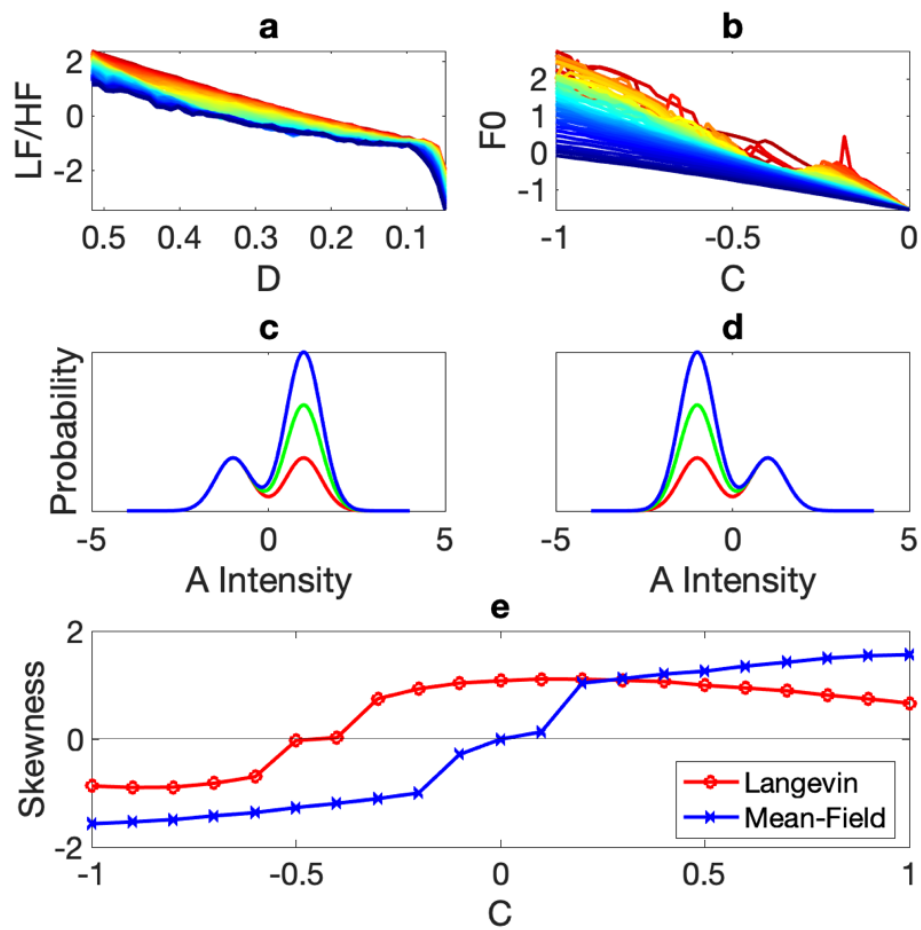


Figure 5

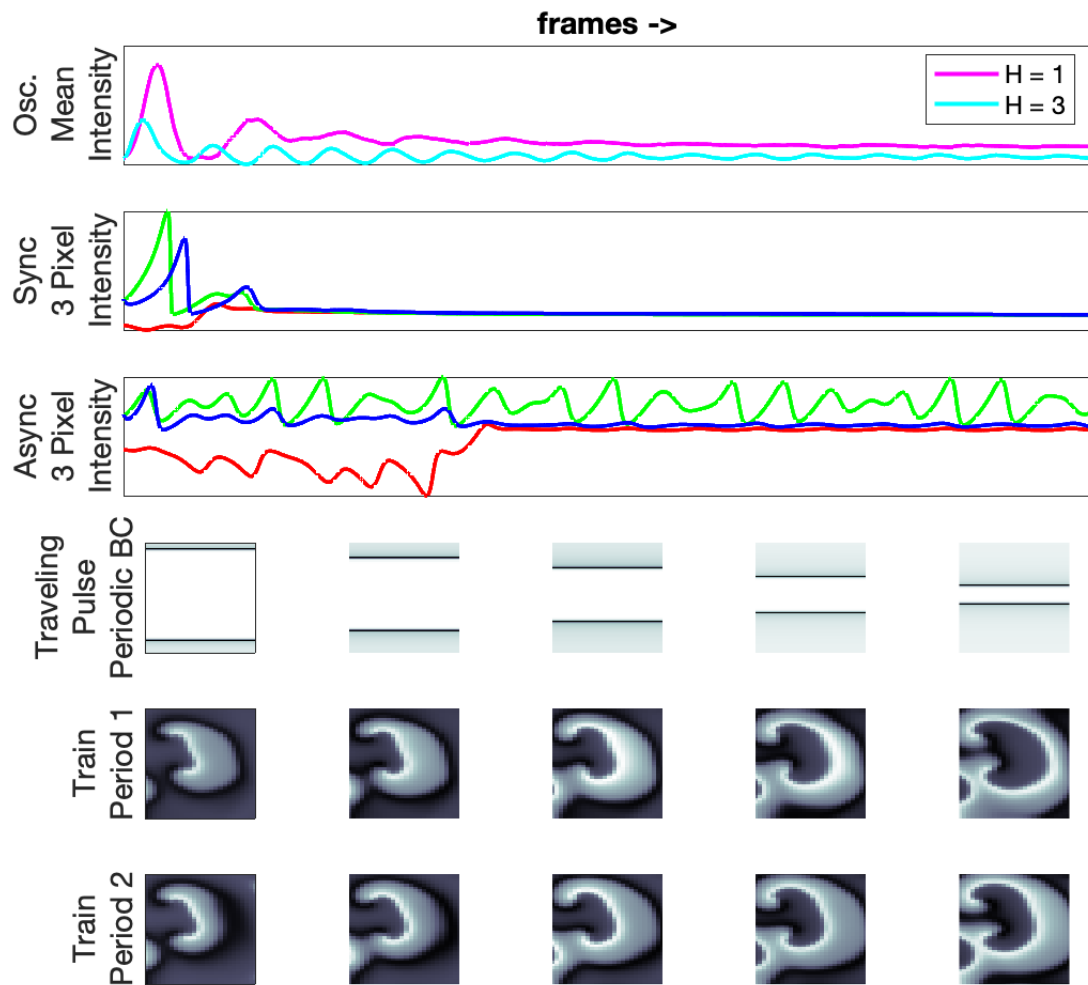


Table 1

	Figure	a	b	g	C	H	D
Stripes	1a	1.112	-1.01	.07	0	-1	.516
Irreg. Stripes	1b	1.112	-1.01	.07	-.2	-1	.44
Stripes + Spots	1c	1.112	-1.01	.07	-.125	-1	.516
Light Spots	1d	1.112	-1.01	.07	-1	-1	.516
Dark Spots	1e	1.112	-1.01	.07	1	-1	.516
Reticulate	2a	1.112	-1.01	.07	-.16	-1	.15
Light Irreg. Spots (Blotch)	2b	1.112	-1.01	.07	-.9	-1	.15
Dark Irreg. Spots (Blotch)	2c	1.112	-1.01	.07	.9	-1	.15
Dark Mottle	2d	1.112	-1.01	.07	-.56	-1	.06
Light Mottle	2e	1.112	-1.01	.07	0	-1	.06
Uniform Light	2f	0	0	0	0	0	1
Uniform Dark	2g	0	0	0	0	0	1
Synchronous Oscillation	5b	1	-1	.4	-1	1	.112
Asynchronous Oscillation	5c	1	-1	.4	-1	3	.112
Traveling Pulse	5d	1	-1	.4	-1	1	.112
Periodic Wave Train	5e,f	-1	1	.2	-.6	3.3	.2

References

- Anderson, J.C., Baddeley, R.J., Osorio, D., Shashar, N., Tyler, C.W., Ramachandaran, V. S., Crook, A.C., and Hanlon, R.T. (2003). Modular organization of adaptive colouration in flounder and cuttlefish revealed by independent component analysis. *Network: Computation in Neural Systems*, 14, 2, 321-333.
- Asai, R., Taguchi, R., Kume Y., Saito, M., and Kondo, S. (1999). Zebrafish Leopard gene as a component of putative reaction-diffusion system. *Mechanisms of Development*, 89, 87–92.
- Bard, J. (1981). A model generating aspects of zebra and other mammalian coat patterns. *Journal of Theoretical Biology*, 93, 2, 363-385.
- Barrio, R. A., Varea, C., Aragón, J. L., and Maini, P. K. (1999). Two-dimensional numerical study of spatial pattern formation in interacting Turing systems. *Bulletin of Mathematical Biology*, 61, 483.
- Bernstein, N. (1967). *The Coordination and Regulation of Movement*. Pergamon.
- Borrelli, L., Gherardi, F., and Fiorito, G. (2006). *A Catalogue of Body Patterning in Cephalopoda*. Firenze University Press.
- Boettiger, A., Ermentrout, B., and Oster, G. (2009). The neural origins of shell structure and pattern in aquatic mollusks. *Proceedings of the National Academy of Sciences*, 106, 16, 6837-6842.
- Browman, C. and Goldstein, L. (1989). Articulatory gestures as phonological units. *Phonology*, 6, 201-251.
- Buice, M. A. and Cowan, J. (2009). Statistical mechanics of the neocortex. *Progress in Biophysics and Molecular Biology*, 99, 53-86.
- Chiao, C.-C., Chubb, C., Buresch, K. C., Barbosa, A., Allen, J. J., Mäthger, L. M., and Hanlon, R. T. (2010). Mottle camouflage patterns in cuttlefish: Quantitative characterization and visual background stimuli that evoke them. *Journal of Experimental Biology*, 213, 2, 187-199.
- Chua, L.O. (2005). Local activity is the origin of complexity. *International Journal of Bifurcation and Chaos*, 15, 11, 3435–3456
- Chung, W.-S., Kurniawan, N. D., and Marshall, J. (2020). Toward an MRI-Based Mesoscale Connectome of the Squid Brain. *iScience*, 23, 100816.
- Cott, H.B. (1940). *Adaptive Coloration in Animals*. Methuen.
- Cooper, R., Thiery, A., Fletcher, A., Delbarre, D., Rasch, L., and Fraser, G. (2018). An ancient Turing-like patterning mechanism regulates skin denticle development in sharks. *Science Advances*, 4.
- Cowan, J. (2014). A personal account of the development of the Field Theory of large-scale brain activity from 1945 onward. In S. Coombs et al. (eds.), *Neural Fields*, (pp. 47-96). Springer-Verlag.
- Cross, M. and Hohenberg, P. (1993). Pattern formation outside of equilibrium. *Reviews of Modern Physics*, 65, 851-1112.
- Dayan, P. and Abbott, A.F. (2001). *Theoretical Neuroscience: Computational and Mathematical Modelling of Neural Systems*. MIT Press.
- De Wit, A. (1999). Spatial patterns and spatiotemporal dynamics in chemical systems. *Advances in Chemical Physics*, 109, 435-513.

- Ermentrout, B., Campbell, J., and Oster, G. (1986). A model for shell patterns based on neural activity. *The Veliger*, 28, 4, 369-388.
- Ermentrout, B. (1991). Stripes or spots? Nonlinear effects in bifurcation of reaction-diffusion equations on the square. *Proceeding of the Royal Society of London, Series A*, 434, 413–417.
- Ermentrout, G. and Cowan, J. (1979). A mathematical theory of visual hallucination patterns. *Biological Cybernetics*, 34, 137-150.
- Fernández-Ruiz, A., Oliva, A., and Soula, M. (2021). Gamma rhythm communication between entorhinal cortex and dentate gyrus neuronal assemblies. *Science*, 372, 6537, eabf3119.
- Fowler, C. A., Rubin, P., Remez, R., and Turvey, M. (1980). Implications for speech production of a general theory of action. In B. Butterworth (ed.), *Langage production, Vol.1: Speech and talk* (pp. 373-420). Academic.
- Hanlon, R.T., Chiao, C.-C., Mäthger, L.M., Barbosa, A., Buresch, K.C., and Chubb, C. (2009). Cephalopod dynamic camouflage: bridging the continuum between background matching and disruptive colouration. *Philosophical Transactions of the Royal Society of London B Biological Sciences*, 364, 1516, 429-437.
- Hanlon, R. and Messenger, J. (1988). Adaptive coloration in young cuttlefish (*Sepia officinalis* L.): The morphology and development of body patterns and their relation to behaviour. *Philosophical Transactions of the Royal Society of London B Biological Sciences*, 320, 1200, 437-487.
- Hanlon, R. and Messenger, J. (2018). *Cephalopod Behaviour* (2nd ed.). Cambridge University Press.
- How, M., Norman, M., Finn, J., Chung, W-S., and Marshall, N. J. (2017). Dynamic Skin Patterns in Cephalopods. *Frontiers in Physiology*, 8, 393.
- Inaba, M. and Chuong, C-M. (2020). Avian Pigment Pattern Formation: Developmental Control of Macro-(Across the Body) and Micro-(Within a Feather) Level of Pigment Patterns. *Frontiers in Cell and Developmental Biology*, 8, 620.
- Ishida, T. (2021). A model of octopus epidermis pattern mimicry mechanisms using inverse operation of the Turing reaction model. *PLOS ONE* 16(8): e0256025
<https://doi.org/10.1371/journal.pone.0256025>.
- Iskarous, K. (2019). The morphogenesis of speech gestures: From local computations to global patterns. *Frontiers in Psychology*, 10, 2395.
- Jaffe, L. (2008). Calcium waves. *Philosophical Transactions of the Royal Society of London B Biological Sciences*, 12, 363, 1311-1316.
- Keener, J. and Sneyd, J. (2001). *Mathematical Physiology*. Springer-Verlag.
- Kelman, E., Tiptus, P., and Osorio, D. (2006). Juvenile plaice (*Pleuronectes platessa*) produce camouflage by flexible combining of two separate patterns. *The Journal of Experimental Biology*, 209, 3288-3292.
- Kondo, S. and Asai, R. (1995). A reaction-diffusion wave on the marine angelfish *Pomacanthus*. *Nature*, 376, 765–768.
- Laan, A., Gutnick, T., Kuba, M. J., and Laurent, G. (2014). Behavioral analysis of cuttlefish traveling waves and its implications for neural control. *Current Biology*, 24, 15, 1737– 1742.
- Leite, T., and Mather, J. (2008). A new approach to octopuses' body pattern analysis: A framework for taxonomy and behavioral studies. *American Malacological Bulletin*, 24, 1, 31-41.
- Leppänen, T., Karttunen, M., Barrio, R., and Kaski, K. (2003). Spatio-temporal dynamics in a Turing model. In Minai et al. (eds.) *Unifying Themes in Complex Systems* (pp. 215-223). Springer.

- Leppänen, T. (2004). *Computational Studies of Pattern Formation in Turing Systems*. Helsinki University of Technology, Dissertation.
- Levy, G., and Hochner, B. (2017). Embodied organization of *Octopus vulgaris*: morphology, vision, and locomotion. *Frontiers in Physiology*, 8, 5.
- Liu, R-T, Liaw, S-S, and Maini, P. (2007). Oscillatory Turing patterns in a simple reaction-diffusion system. *Journal of the Korean Physical Society*, 50, 1, 234-238.
- Liu, T.-H., and Chiao, C.-C. (2017). Mosaic organization of body pattern control in the optic lobe of squids. *Journal of Neuroscience*, 37, 4, 768–780.
- Marquez-Lago, T.T. and Padilla, P. (2014). A selection criterion for patterns in reaction–diffusion systems. *Theoretical Biology and Medicine Modeling*, 11, 7, 2014.
- Mather, J. and Alupay, J. S. (2016). An ethogram for benthic Octopods (Cephalopoda: Octopodidae). *Journal of Comparative Psychology*, 130, 2, 109-127.
- Mather, J. A. and Mather, D.L. (2004). Apparent movement in a visual display: The ‘Passing Cloud’ of *Octopus cyanea* (Mollusca: Cephalopoda). *Journal of Zoology*, 263, 89-94.
- Maxwell, J. C. (1871). Remarks on the mathematical classification of physical quantities. *Proceedings of the London Mathematical Society*, s1-3, 224-233.
- Meinhardt, H. (1982) *Models of Biological Pattern Formation*. Academic.
- Meinhardt, H. (2012). Turing’s theory of morphogenesis of 1952 and the subsequent discovery of the crucial role of local self-enhancement and long-range inhibition. *Interface Focus*, 2, 407-416.
- Melloni, L., Molina, C., Pena, M., Torres, D., Singer, W., and Rodriguez, E. (2007). Synchronization of Neuronal Activity across Cortical Areas Correlates with Conscious Perception. *The Journal of Neuroscience*, 27, 11, 2858-2865.
- Messenger, J. B. (2001). Cephalopod chromatophores: Neurobiology and natural history. *Biological Reviews*, 76, 473–528.
- Murray, 2001. *Mathematical Biology*, 3rd ed. Springer.
- von Neumann, J. (1956). Lectures on probabilistic logics and the synthesis of reliable organisms from unreliable components. In C. Shannon (ed.), *Automata Studies* (pp. 43-98). Princeton University Press.
- Newman, S. (2019). Inherency and homomorphy in the evolution of development. *Current Opinions in Genetics and Development*, 57, 1-6.
- Norman, N. and Debelius, H. (2000). *Cephalopods: A World Guide*. Conchbooks.
- Osorio, D. (2014). Cephalopod Behaviour: Skin Flicks. *Current Biology*, 24, 15, 684-685.
- Oster, G. (1988). Lateral inhibition models of developmental processes. *Mathematical Biosciences*, 90, 265-286.
- Packard, A. (1995). Through the looking-glass of cephalopod colour patterns. In E. Alleva, A. Fasolo, H-P. Lipp, L. Nadel, and L. Ricceri (eds.) *Behavioural Brain Research in Naturalistic and Semi-Naturalistic Settings* (pp.105-130). NATO Series.
- Packard, A. (2001). A ‘neural’ net that can be seen with the naked eye. In International School of Biocybernetics (Ischia): In W. Backhaus (ed.) *Neuronal coding of perceptual systems* (pp. 397-402). World Scientific.
- Packard, A. (2006). Contribution to the whole. Can squids show us anything that we did not know already? *Biology and Philosophy*, 21, 189-211.
- Packard, A. and Sanders, G. (1969). What the octopus shows to the world. *Endeavour*, 28, 104, 92-99.

- Packard, A. and Sanders, G. (1971) Body patterns of *Octopus vulgaris* and maturation of the response to disturbance. *Animal Behaviour*, 19, 780-790.
- Plummer, B. N., Cutler, M. J., Wan, X., and Laurita, K. (2011). Spontaneous calcium oscillations during diastole in the whole heart: the influence of ryanodine reception function and gap junction coupling. *American Journal of Physiology- Heart and Circulatory Physiology*, 300, H1822-H1828.
- Reiter, S., Hülndunk, P., Woo, T., Lauterbach, M., Eberle, J., Akay, L., Longo, A., Meier-Credo, J., Kretschmer, F., Langer, J., Kaschube, M., and Laurent, G. (2018). Elucidating the control and development of skin patterning in cuttlefish. *Nature*, 562, 361-366.
- Rosen, H., Gilly, W., Bell, L., Abernathy, K. and Marshall, G. (2015). Chromogenic behaviors of the Humboldt squid (*Dosidicus gigas*) studied in situ with an animal-borne video package. *Journal of Experimental Biology*, 218, 265-275.
- Rosen, H. and Gilly, W. (2017). Myogenic activity and serotonergic inhibition in the chromatophore network of the squid *Dosidicus gigas* (family Ommastrephidae) and *Doryteuthis opalescens* (family Loliginidae). *Journal of Experimental Biology*, 220, 4669-4680.
- Saltzman, E., and Munhall, K. (1989). A dynamical approach to gestural patterning in speech production. *Ecological Psychology*, 1, 333-382.
- Shoji, H., Iwasa, Y. and Kondo, S. (2003) Stripes, spots, or reversed spots in a two-dimensional Turing system. *Journal of Theoretical Biology*, 224, 3, 339-50.
- Shoji, H. and Iwasa, Y. (2003). Pattern selection and the direction of stripes in two-dimensional Turing systems for skin pattern formation of fishes. *Forma*, 18, 3-18.
- Sorenson, T., and Gafos, A. (2016). The gesture as an autonomous nonlinear dynamical system. *Ecological Psychology*, 28, 188-215.
- Sumbre, G., Gutfreund, Y., Fiorito, G., Flash, T., and Hochner, B. (2001). Control of octopus arm extension by a peripheral motor program. *Science*, 293, 7, 1845-1848.
- Turing, A. (1952), The chemical basis of morphogenesis, *Philosophical Transactions of the Royal Society of London, Series B, Biological Sciences*, 237, 37-72.
- Turvey, M. (1990). Coordination. *American Psychologist*, 45, 8, 938-953.
- Varea, C., Hernández, D., and Barrio, R.A. (2007). Soliton behavior in a bistable reaction diffusion model. *Journal of Mathematical Biology*, 54, 797-813.
- Walgraef, D. (1997). *Spatio-temporal pattern formation: With examples from Physics, Chemistry, and Material Science*. Springer.
- Watanabe, M. and Kondo, S. (2015). Is pigment patterning in fish skin determined by the Turing mechanism? *Trends in Genetics*, 31, 2, P86-96.
- Wilson, H. and Cowan, J. (1972). Excitatory and Inhibitory Interactions in localized populations of model neurons. *Kybernetik*, 13, 55-80.
- Wilson, H. and Cowan, J. (1973). A mathematical theory of the functional dynamics of cortical and thalamic nervous tissue. *Biophysical Journal*, 12, 1, 1-24.
- Zemel, R., Dayan, P., and Pouget, A. (1998). Probabilistic interpretation of population codes. *Neural Computation*, 10, 403-430.
- Zylinski, S., How, M.J., Osorio, D., Hanlon, R.T., and Marshall, N.J. (2011). To be seen or to hide: visual characteristics of body patterns for camouflage and communication in the Australian giant cuttlefish *Sepia apama*. *American Naturalist*, 177, 5, 681-690.

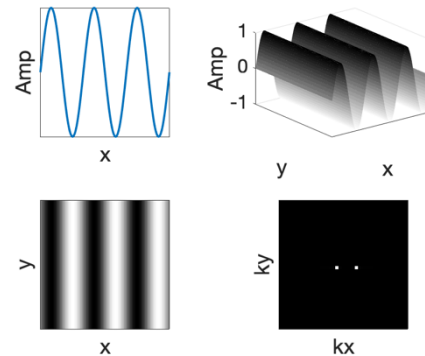
Appendix A: Numerical Reaction-Diffusion Simulations

We followed Barrio et al. (1999) and Varea et al. (2007) in using Euler's explicit method for simulating the BVAM reaction-diffusion equations. For Figure 1 and 2, the spatial domain was discretized into a 200x200 grid, with $dt = .1$. Each simulation was run for 500,000 iterations, and the initial conditions were initiated with Gaussian noise with mean 0 and standard deviation .01. The coefficients used are given in Table 1. We used periodic boundary conditions, which is unusual, since most previous studies have used zero-flux boundary conditions. de Witt (1996) showed, however, that unless the dx is very small, which is problematic for stability, zero-flux boundary conditions introduce significant artifacts to the pattern, whereas periodic boundary conditions don't.

For Figure 3, the domain of C was -1 to 0 and the domain of D was .05 to .516, and each were discretized into 50 steps, therefore 2500 simulations were run. The values of the coefficients other than C and D were fixed at the values in Table 1. The spatial domain was discretized into a 64x64 grid, with $dt = .25$. The same random initial conditions were used for all simulations. Figure 3 was computed by converting each pattern matrix to a vector, and then running k-means clustering on the vectors with Euclidean metric, and the specification of 6 clusters. One color was used, arbitrarily for each cluster.

Appendix B: 2D Fourier Transform

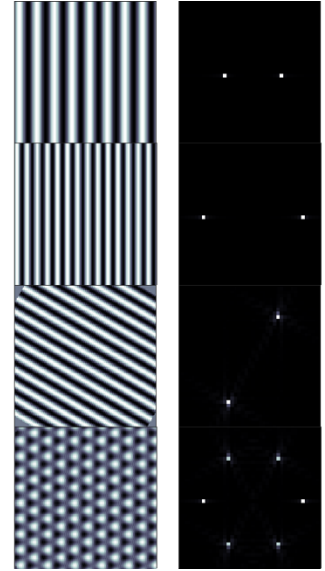
The one-dimensional Fourier transform centers around sinusoids, and tries to find the frequency context of signals. The top left panel of Figure SIB1 shows a sinusoid with three peaks (3Hz) on a spatial domain x . If a 2D spatial domain has that same sinusoidal variation on coordinate x , but is



constant, for each x , along y , then we can represent the variation in the amplitude using the top right panel. Seen as a relief, we get the bottom left display, where dark color is high amplitude, and light color is low amplitude. In one dimension, the Fourier spectrum will have one positive and one negative peak. The 2D Fourier Spectrum, also called k -space, shown in the bottom right panel, will have peaks in the x -direction, seen as two light spots. But it will not have peaks in the y -direction, as there is no variation in y . Note that stripes, or lines, are the simplest kind of pattern from the 2D Fourier perspective, in the same way that a sinusoid is the basic signal in 1D.

Figure SIB2 top row shows the pattern (left) and 2D Fourier Transform (right) for stripes again. If the spatial frequency of stripes rises, as seen in row 2, the 2D spectral peaks travel outwards. If the stripes are tilted, so are the peaks in the spectrum, as seen in the third row. Therefore, the radial location in the 2D spectrum represents the frequency of variation, whereas the

angular direction represents the tilt of the pattern. More complex patterns can be built from stripes. So, if three sets of stripes at 0 degrees, 60 degrees, and 120 degrees are added, the superposition of the peaks and troughs would align in such a way as to produce spots, as in the lowest row. It can be seen from this exposition that as D falls in the equations, the 2D spectrum will have more and more peaks as we travel outwards. As C rises in magnitude towards -1, the more peaks there will be near some circle. Therefore, the Fourier 2D spectrum, which can be easily computed from real patterns, directly reveals the two main parameters, C and D , of the underlying reaction-diffusion equations.



Appendix C: Fokker-Planck Simulation

To obtain the pattern-selection histograms in the fourth column of Figures 1 and 2, the Fokker-Planck equations were simulated via the Langevin method. In this method, the BVAM equations become:

$$\begin{aligned}dA &= g(A + aI - CAI - AI^2) + D_A \zeta_A \sqrt{dt} \\dI &= g(HA + bI + CAI + AI^2) + \zeta_I \sqrt{dt}\end{aligned}$$

Where ζ is white noise. So, space has disappeared, and has been replaced by a gaussian noise process whose variance is the diffusion coefficient, and whose bias is the reaction portion of BVAM, with $dt = .01$. For each panel of column 4 of Figures 1 and 2, 10000 simulations were done, and the panels show the histograms of A for each combination of parameters.